Supporting Information

Self-Assembly of Peptide Hierarchical Helical Arrays with Sequence-Encoded Circular Polarized Luminescence

Qing Li,[†, ‖] *Jiaxing Zhang,*[†, ‖] *Yuefei Wang,*[†, §, *] *Gong Zhang,*[†] *Wei Qi,*[†, ‡, §] *Shengping You,*[†, §] *Rongxin Su,*[†, ‡, §] *Zhimin He*[†]

[†]School of Chemical Engineering and Technology, State Key Laboratory of Chemical Engineering, Tianjin University, Tianjin 300072, P. R. China

[‡]Collaborative Innovation Center of Chemical Science and Engineering (Tianjin), Tianjin 300072, P. R. China

[§]Tianjin Key Laboratory of Membrane Science and Desalination Technology, Tianjin University, Tianjin 300072, P. R. China.

[‖] These authors contributed equally to this work.

*Correspondence: wangyuefei@tju.edu.cn

Materials

N-(9-fluorenylmethoxycarbonyl)-$_L$-phenylalanine-$_L$-tryptophan-$_L$-serine (Fmoc-$_L$-FWS, >98%), N-(9-fluorenylmethoxycarbonyl)-$_D$-phenylalanine-$_D$-tryptophan-$_D$-serine (Fmoc-$_D$-FWS, >98%), N-(9-fluorenylmethoxycarbonyl)-$_L$-phenylalanine-$_L$-phenylalanine-$_L$-serine (Fmoc-FFS, >98%), N-(9-fluorenylmethoxycarbonyl)-$_L$-phenylalanine-$_L$-tryptophan-$_L$-lysine (Fmoc-$_L$-FWK, >98%), N-(9-fluorenylmethoxycarbonyl)-$_L$-phenylalanine-$_L$-phenylalanine-$_L$-lysine (Fmoc-$_L$-FFK, >98%), N-(9-fluorenylmethoxycarbonyl)-$_L$-phenylalanine-$_L$-tryptophan-$_L$-arginine (Fmoc-$_L$-FWR, >98%), and N-(9-fluorenylmethoxycarbonyl)-$_L$-phenylalanine-$_L$-phenylalanine-$_L$-arginine (Fmoc-$_L$-FFR, >98%) were synthesized from GL Biochem Ltd. (Shanghai, China); (R)-(−)-2-methylpiperazine, (S)-(+)-2-methylpiperazine, and Thioflavin T were purchased from Sigma-Aldrich (Shanghai, China); Coumarin 6, and Acid Red 52 were purchased from J&K Scientific Ltd. (Beijing, China); Sodium hydroxide, Tetraphenylethylene, and 1,1,1,3,3,3-hexafluoro-2-propanol (HFIP) were purchased from the Aladdin Reagent Corporation (Shanghai, China).

Preparation of the Fmoc-Tripeptide Hierarchical Helical Arrays.

To prepare the Fmoc-tripeptide hierarchical helical arrays, we first dissolved the Fmoc-$_L$-FWS molecules in 1,1,1,3,3,3-hexafluoro-2-propanol (HFIP), a highly polar solvent, at a concentration of 1.42 mol L^{-1} and dissolved the (S)-(+)-2-methylpiperazine molecules in 1,1,1,3,3,3-hexafluoro-2-propanol (HFIP) at a concentration of 4 mol L^{-1} at 20 °C. Then, 5 μL of (S)-(+)-2-methylpiperazine solutions were added to 35 μL of Fmoc-$_L$-FWS solutions. After shaking for 1.5 min, the mixtures were allowed to stand for 30 minutes at 20 °C. Then, 10 μL of the solutions were dropped on a glass substrate. The sample was placed in the vacuum desiccator and vacuumed for 2 minutes to form the amorphous film. Finally, The glass was stuck on the top of a chromatographic bottle then put the

bottle in a screw-cap vial involving 3 ml ddH_2O. The thin films were further annealed at 80 °C for 12 h without any disturbance. For the other Fmoc-tripeptides or the other ratio of the Fmoc-tripeptide/2-methylpiperazine, the peptide assemblies were obtained following the similar preparation procedure of Fmoc-$_L$-FWS as described above.

Preparation of the Peptide Films with the Circularly Polarized Luminescence.

To prepare the Fmoc-tripeptide films with the circularly polarized luminescence, we first dissolved the Fmoc-$_L$-FWS molecules in 1,1,1,3,3,3-hexafluoro-2-propanol (HFIP), at a concentration of 1.42 mol L^{-1}, the (S)-(+)-2-methylpiperazine molecules in 1,1,1,3,3,3-hexafluoro-2-propanol (HFIP) at a concentration of 4 mol L^{-1}, and Thioflavin T molecules in 1,1,1,3,3,3-hexafluoro-2-propanol (HFIP) at a concentration of 0.029 mol L^{-1}at 20 °C. Then, 5 μL of (S)-(+)-2-methylpiperazine solutions were added to 35 μL of Fmoc-$_L$-FWS solutions. After shaking for 1.5 min, 1.5 μL Thioflavin T solutions were added to the mixed solutions of Fmoc-$_L$-FWS and (S)-(+)-2-methylpiperazine. And the mixtures were allowed to stand for 30 minutes at 20 °C after shaking for 1.5 min. Then, 10 μL of the solutions were dropped on a glass substrate. The sample was placed in the vacuum desiccator and vacuumed for 2 minutes to form the amorphous film. Finally, The glass was stuck on the top of a chromatographic bottle then put the bottle in a screw-cap vial involving 3 ml ddH_2O. The thin films were further annealed at 80 °C for 12 h without any disturbance. For the other Fmoc-tripeptide or the achiral fluorescent molecules, the peptide assemblies were obtained following the similar preparation procedure of Fmoc-$_L$-FWS with Thioflavin T as described above. However, the tetraphenylethylene was dissolved in the dichloromethane.

Preparation of the Peptide Aqueous Solutions Containing Various Peptides and Dyes.

To prepare the Fmoc-tripeptide solutions containing various peptides and dyes, we first dissolved the Fmoc-$_L$-FWS molecules in 1,1,1,3,3,3-hexafluoro-2-propanol (HFIP) at a concentration of 1.42 mol L^{-1}, the (S)-(+)-2-methylpiperazine molecules in HFIP at a concentration of 4 mol L^{-1}, and Thioflavin T molecules in HFIP at a concentration of 0.029 mol L^{-1} at 20 °C. Then, 5 μL of (S)-(+)-2-methylpiperazine HFIP solution were added to 35 μL of Fmoc-$_L$-FWS HFIP solution. After shaking for 1.5 min, 1.5 μL Thioflavin T HFIP solution was added to the mixed HFIP solution of Fmoc-$_L$-FWS and (S)-(+)-2-methylpiperazine. Finally, 10 μL of the resulting mixture solution was added into 990 μL ddH_2O. For the other Fmoc-tripeptide with the achiral fluorescent molecules, the aqueous solutions were obtained following the similar preparation procedure of Fmoc-$_L$-FWS with Thioflavin T as described above.

Molecular Dynamics Simulation.

The MD simulation was performed with Gromacs 2019.6 software package [1] under Amber99SB-ildn force field [2]. The structures containing 48 Fmoc-$_L$-FWS or Fmoc-$_L$-FFS molecules were constructed with PyMOL [3]. Then the boxes were filled with spc water [4], and sodium ions were added into the system to maintain electrical neutrality. Then the energy-minimization stage was performed for 5000 steps with steepest descendant algorithm, followed by production simulation stage for 40 ns under NPT ensemble. The MD simulation trajectories were analyzed with Gromacs tools, Visual Molecular Dynamics [5] and MDAnalysis python package.

Coarse-Grained Molecular Dynamics Simulation.

The CG-MD simulation was performed with Gromacs 2019.6 software package [1] under MARTINI v2.2 force field.[6] The Fmoc-$_L$-FWS, Fmoc-$_L$-FFS and coumarin molecules were firstly pretreated into coarse-grained style, and the corresponding topology files were generated. Then, fifty Fmoc-$_L$-FWS or Fmoc-$_L$-FFS molecules were randomly placed into cubic box with side length of 8 nm, separately, and five coumarin molecules were further added into both systems. Each box was consequently filled with both polarized and unpolarized MARTINI water molecules with a radius of 0.21 nm, and then the system was energy-minimized for 5000 steps with steepest descendant algorithm to reach energy minimum point, and thus undergone CG-MD production simulation for 2 μs under NPT ensemble. The CG-MD simulation trajectories were analyzed with Gromacs tools, Visual Molecular Dynamics [5].

TDDFT Calculation.

Fluorescence of coumarin was calculated with Gaussian 09 [7]. The molecular structures of coumarin were extracted from CG-MD trajectory backward, and geometrically optimized under B3LYP method [8] and 6-31G* basis [9]. The excited states were calculated by Time-Dependent Density Functional Theory (TDDFT) method [10] and 6-311G* basis [9], and fluorescence emission spectrum was analyzed and generated with Multiwfn [11].

Characterization Methods.

The morphologies and structures of the Fmoc-tripeptide self-assemblies were investigated using scanning electron microscopy (SEM, Hitachi S-4800, Japan) at an acceleration voltage of 5 kV. The samples were sputter-coated with platinum using an E1045 Pt-coater (15 mA, 100 s). The structures

of the protofilaments were recorded by using the transmission electron microscopy (TEM, JEM-2100F, Japan) at an acceleration voltage of 200kV. Specifically, the Fmoc-$_L$-FWS film was ultrasonically dispersed in 6 ml ddH_2O. Then, 10 μL of the sample was dropped on the surface of the ultra-thin carbon film carrier screen. After drying, it was stained with a 1% phosphotungstic acid aqueous solution (pH ≈ 6). Circular Dichroism (CD) analysis was employed on a J-810 CD spectropolarimeter (Jasco Inc., Japan). The spectra were collected over a wavelength range of 200–700 nm. The data were recorded with a scanning speed of 500 nm min^{-1} with bandwidth of 2 nm. Circularly Polarized Luminescence (CPL) spectra were obtained by using a CPL-200 (Jasco Inc., Japan). The data were recorded with a scanning speed of 100 nm min^{-1} with bandwidth of 1 nm. The digital integration time (D.I.T.) is 4.0 s with multiple accumulations (15 times or more). Vibrational Circular Dichroism (VCD) and IR spectra were employed on a ChiralIR-2X Fourier transform VCD (FT-VCD) spectrometer (BioTools, Inc, Jupiter, Florida, USA). The data were recorded with the scans per block of 2000 nm over a wavelength range of 500–4000 cm^{-1}. VCD and IR spectra were acquired for 0.5-1 hours at 4 cm^{-1} spectral resolution. In order to eliminate the influence of linear polarization on the authenticity of the test data, we rotated the sample during CD, CPL, and VCD testing. The fluorescence spectrophotometer (Agilent Inc., U.S.) was used for fluorescence analysis of each dye solution: 2 mL sample solution was pipetted into the path-length quartz cuvette. For self-assembly fluorescence, the excitation wavelength was set at 265 nm with a slit of 5 nm, and the emission wavelength was set at 400–800 nm with a slit of 5 nm. All fluorescence spectra were tested at 25°C. Small-angle X-ray diffraction (XRD) measurements were performed using a Smartlab system with a Cu/Kα radiation source (λ = 1.5406 Å) for small angle diffraction (0.5°–5°) with a scanning speed of 0.5° min^{-1}. In situ X-ray scattering measurements were carried out at beamline

1W2A of the Beijing Synchrotron Radiation Facility (Beijing, China). Mar165-CCD was set at 235.6 mm sample–detector distance. The wavelength of the radiation source was $\lambda = 1.54$ Å. The quantum yield of the peptide/coumarin 6 films and isolated coumarin 6 solutions (1mM) were measured using the integrating-sphere method in FLS1000 (Edinburgh Instruments, England). The excitation was set to 350 nm, and the luminescence range was set to 330–700 nm.

Figures

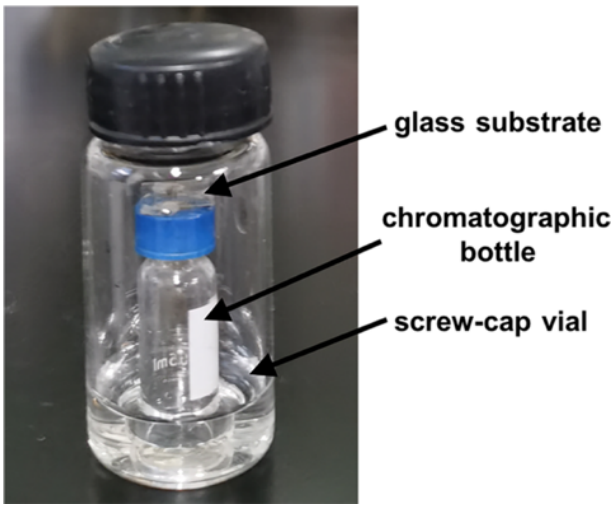

Figure S1. A photograph of the reaction device.

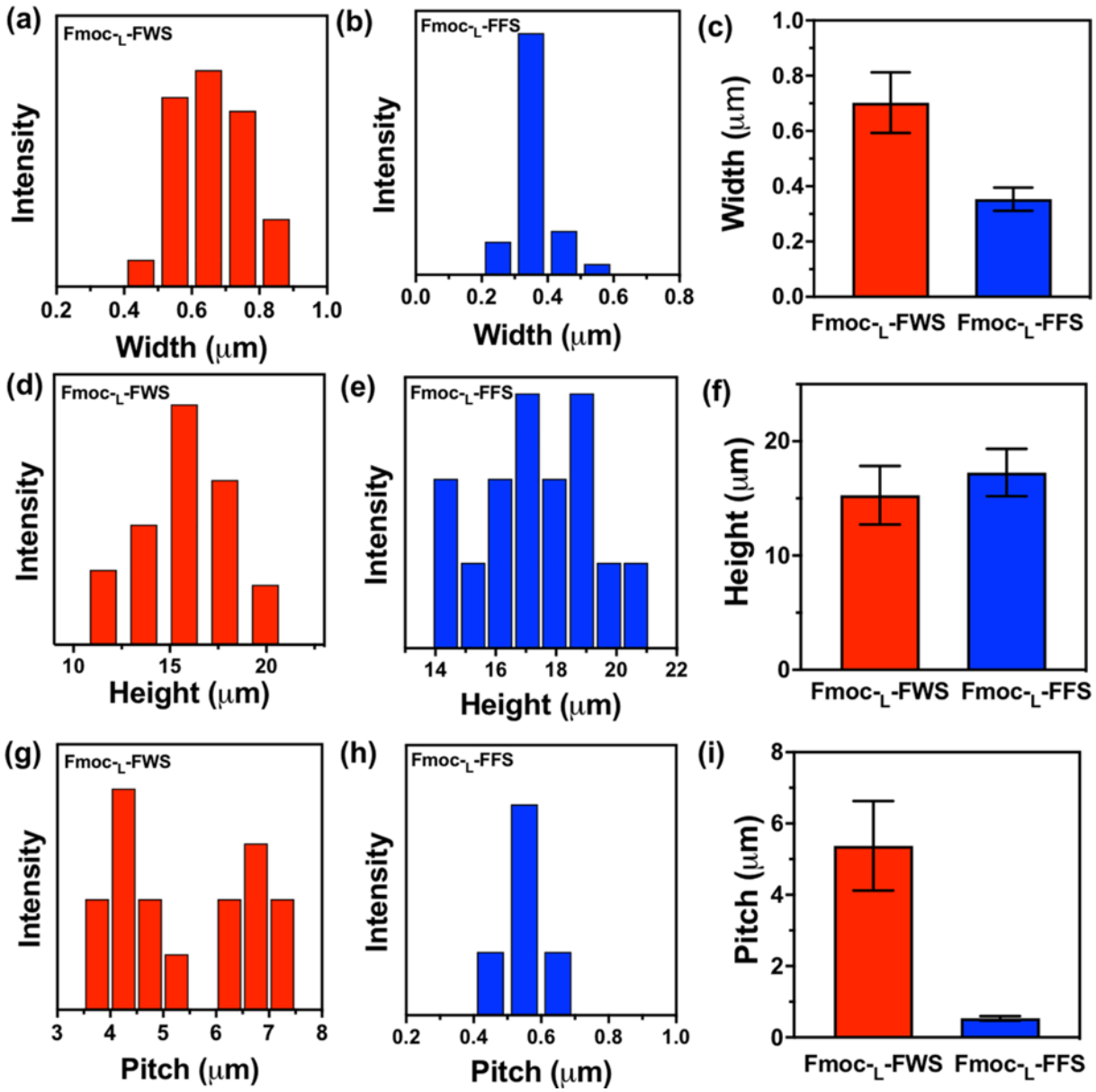

Figure S2. Statistical width, height, and helical pitch of the Fmoc-L-FWS and Fmoc-L-FFS HHAs.

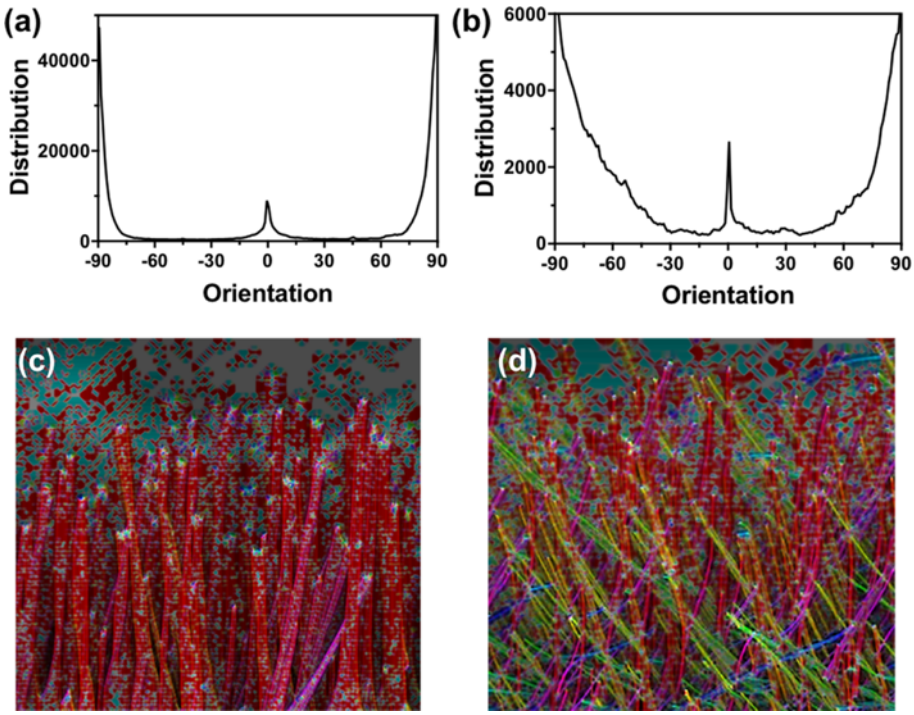

Figure S3. (a, c) Fmoc-$_L$-FWS and (b, d) Fmoc-$_L$-FFS HHAs orientation distribution curves and images.

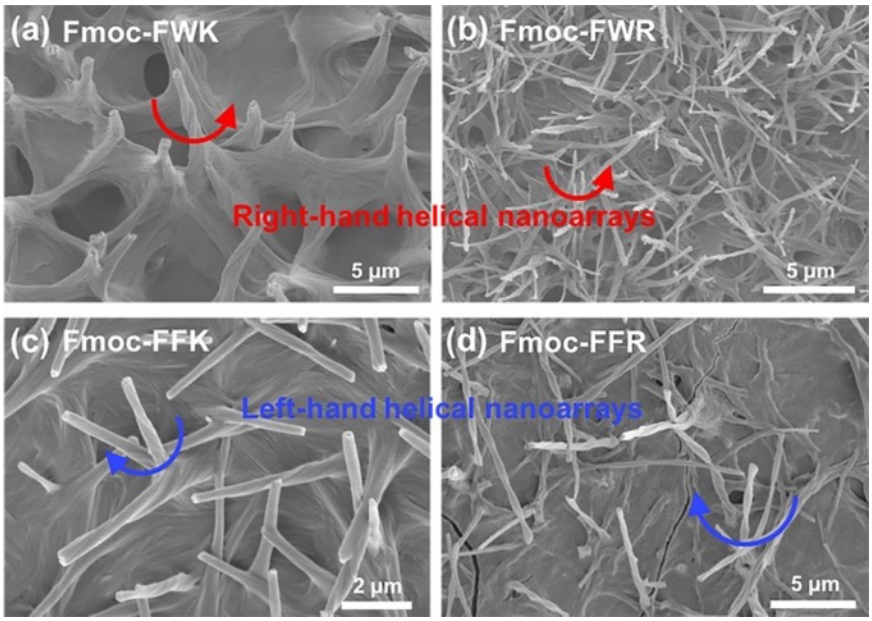

Figure S4. SEM images of the HHAs formed by (a) Fmoc-FWK, (b) Fmoc-FWR, (c) Fmoc-FFK, and (d) Fmoc-FFR with the (S)-(+)-2-Methylpiperazine after water vapor annealing at 80 °C for 12h, respectively.

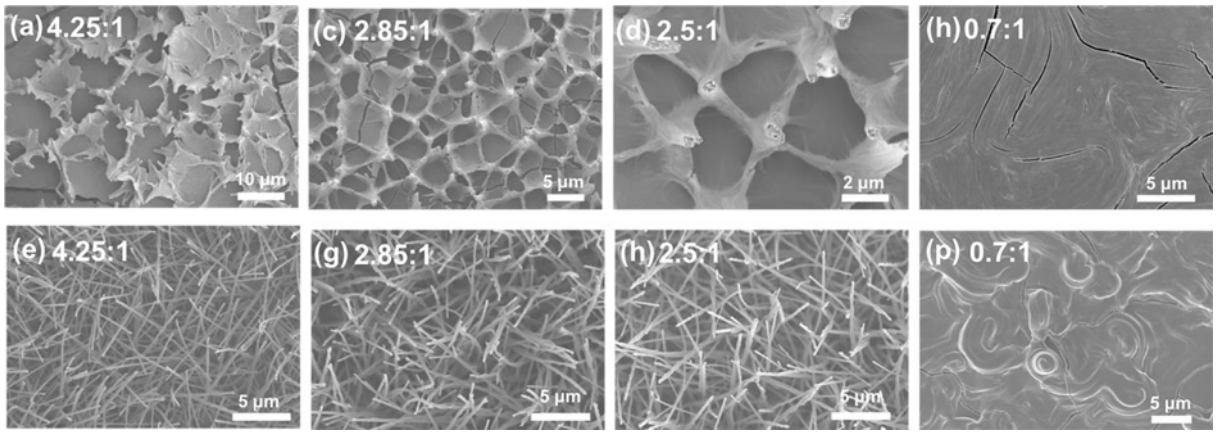

Figure S5. SEM images of the (a-d) Fmoc-$_L$-FWS, and (e-h) Fmoc-$_L$-FFS films formed with different ratios of tripeptide derivatives and (S)-(+)-2-Methylpiperazine after water vapor annealing at 80 °C for 12h, respectively.

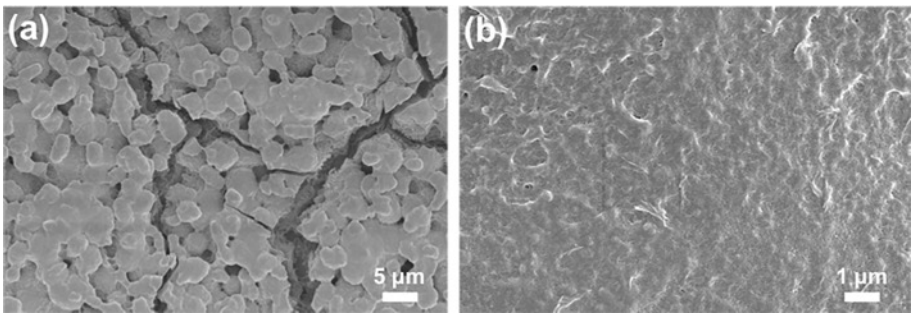

Figure S6. SEM images of the (a) Fmoc-$_L$-FWS and (b) Fmoc-$_L$-FFS films formed without diamines after water vapor annealing at 80 °C for 12h, respectively.

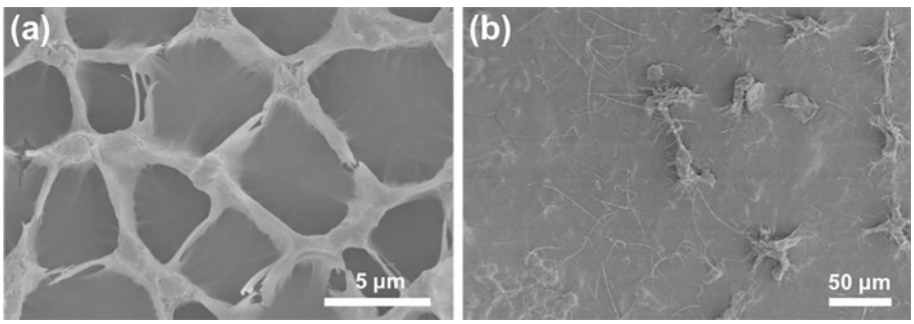

Figure S7. SEM images of the assemblies formed by (a) Fmoc-$_L$-FWS, and (b) Fmoc-$_L$-FFS when the ratio of Fmoc-tripeptide derivatives and (R)-(-)-2-Methylpiperazine was 2.5:1 after water vapor annealing at 80 °C for 12 h, respectively.

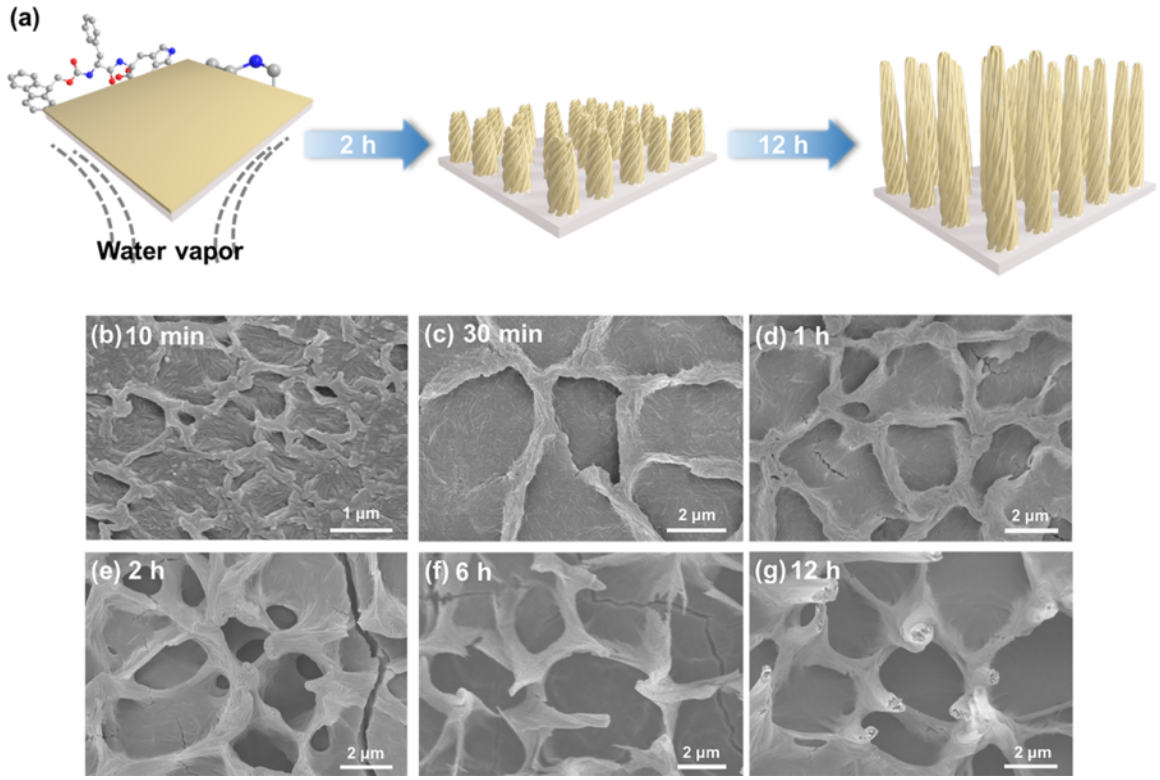

Figure S8. (a) Schematic illustrations of the Fmoc-$_L$-FWS HHAs as a function of incubation time. (b-g) SEM images of the HHAs formed by Fmoc-$_L$-FWS at different incubation time after water vapor annealing at 80 °C.

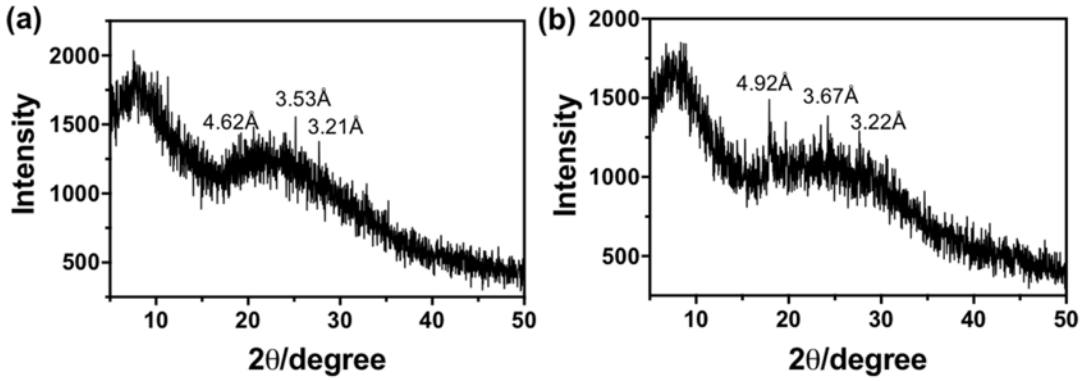

Figure S9. Wide angle X-ray diffraction (WAXD) curves of (a) Fmoc-$_L$-FWS and (b) Fmoc-$_L$-FFS films formed after water vapor annealing at 80 °C for 12 h, respectively.

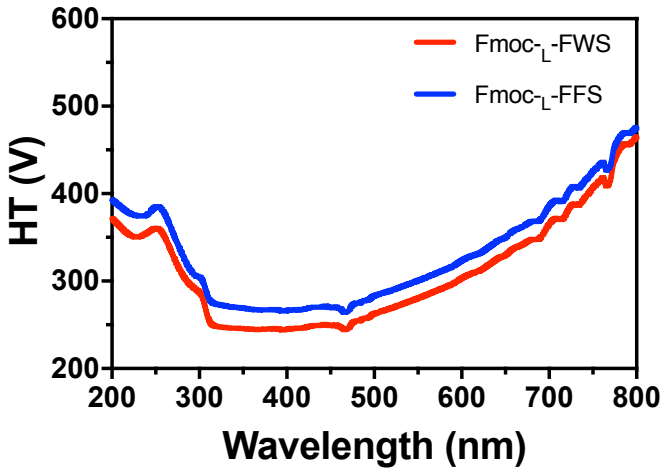

Figure S10. HT spectra of the Fmoc-L-FWS and Fmoc-L-FFS films formed after water vapor annealing at 80 °C for 12 h, respectively.

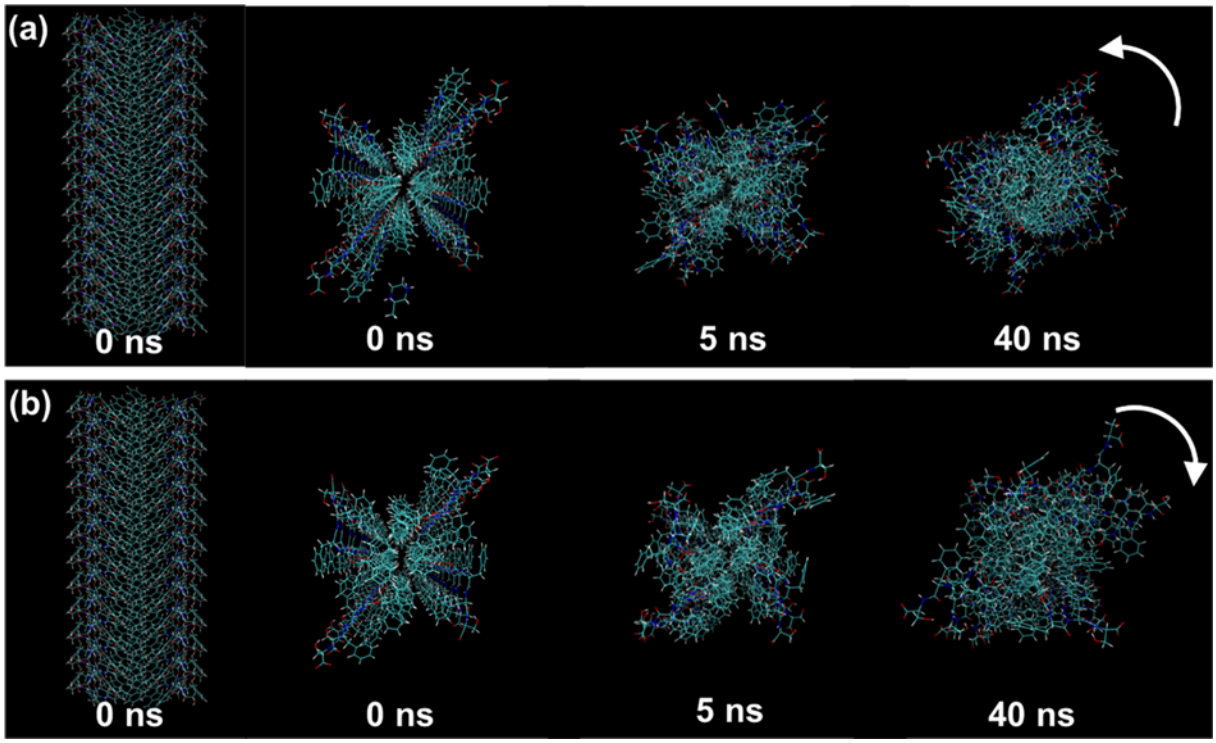

Figure S11. Molecular dynamic simulations of (a) Fmoc-L-FWS self-assembling into right-handed helical arrays and (b) Fmoc-L-FFS self-assembling into left-handed helical arrays.

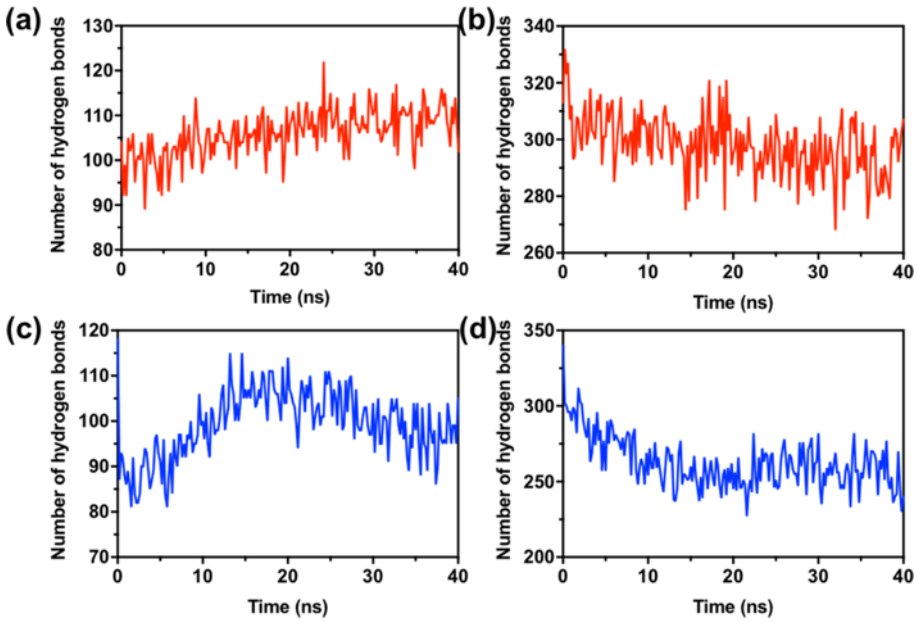

Figure S12. Number of hydrogen bonds during simulation period of (a) Fmoc-L-FWS inside peptide group and (b) between peptide and water, (c) Fmoc-L-FFS inside peptide group and (d) between peptide and water. On the one hand, the five-member ring and the phenyl ring of the indole side chain constituted a bigger steric barrier so that the peptide tend to form a local right-handed secondary structure, leading to the formation of right-handed helical nanostructures. On the other hand, number of hydrogen bonds during the simulation period was analyzed. The side chain of tryptophan in Fmoc-L-FWS contains a nitrogen atom that could form hydrogen bonds with water, and the stronger hydrogen bonding interactions had a vital effect on the handedness during the self-assembly process of Fmoc-L-FWS assemblies, leading to the formation of right-handed helical fibers.

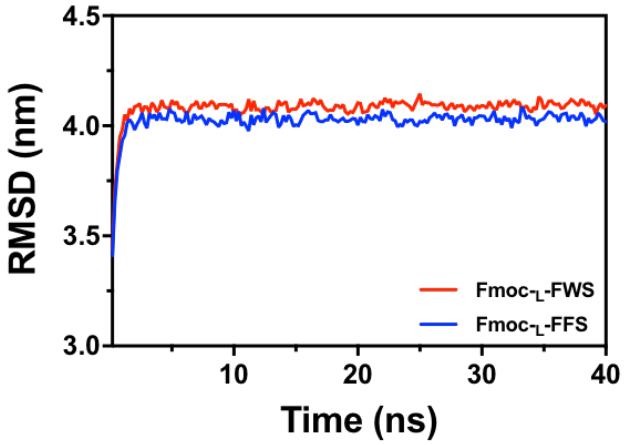

Figure S13. Root Mean Square Deviation (RMSD) during simulation period of Fmoc-L-FWS and Fmoc-L-FFS systems. The Root Mean Square Deviation (RMSD) of each system during the MD simulation period was calculated against simulation time.

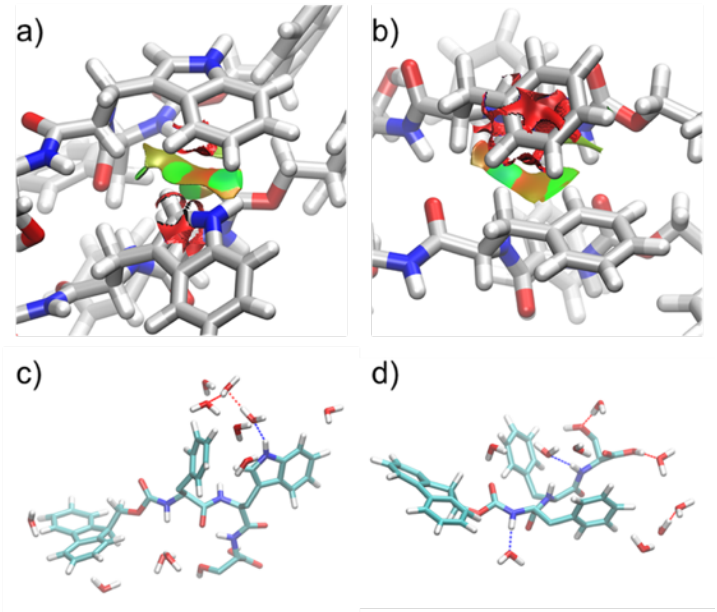

Figure 14. π-π stacking interactions between the side chain of two adjacent (a) Fmoc-L-FWS or (b) Fmoc-L-FFS molecules among two identical layers. Hydrogen bond interactions between the side chains of two adjacent (c) Fmoc-L-FWS or (d) Fmoc-L-FFS molecules. Both mid-position peptides could form hydrogen bonds with water through side chains. The nitrogen atom of tryptophan in Fmoc-L-FWS forms an extra hydrogen bond with a water molecule (as the red arrow indicated). These results showed that aromatic stacking and the hydrogen bond between the side chain and water molecules may play a key role in the assembly behavior.

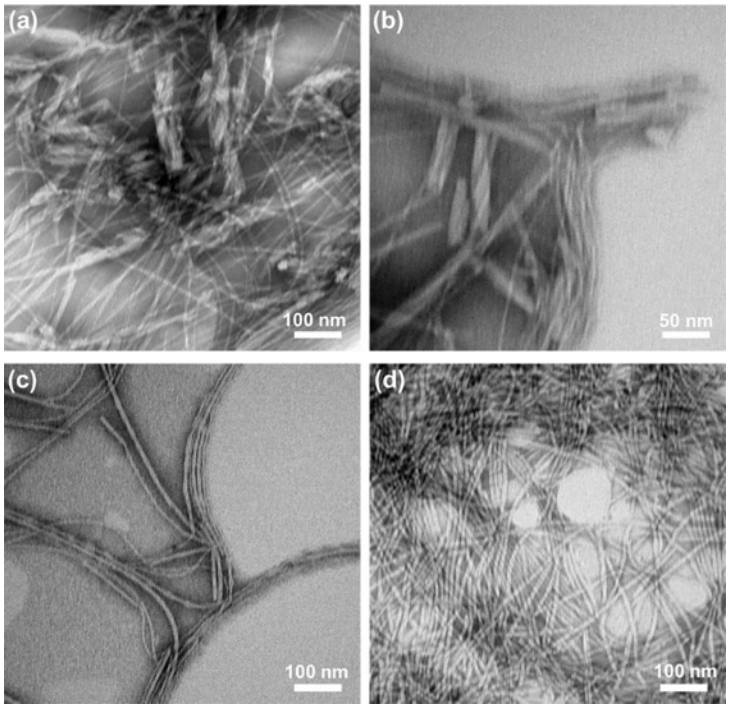

Figure S15. TEM images of the Fmoc-L-FWS right-handed helical fibers assembled after water vapor annealing at 80 °C for 12 h.

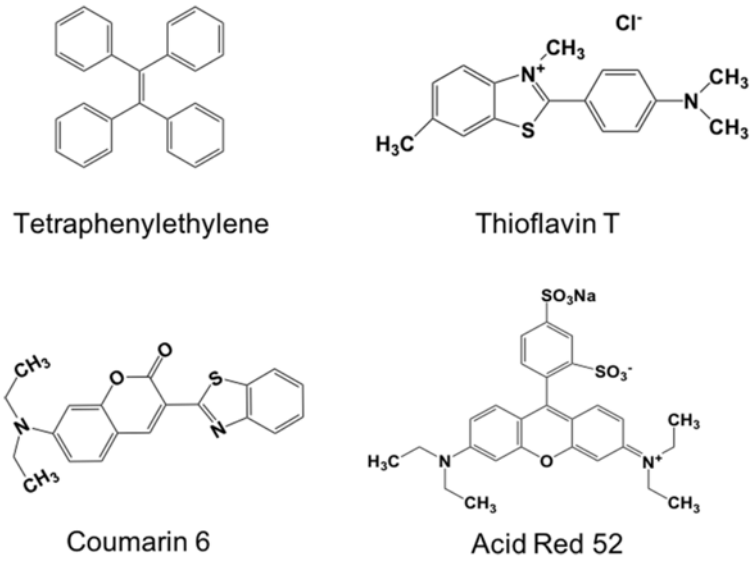

Figure S16. Molecular Structure of the achiral fluorescent molecules: tetraphenylethylene, thioflavin T, coumarin 6, acid red 52.

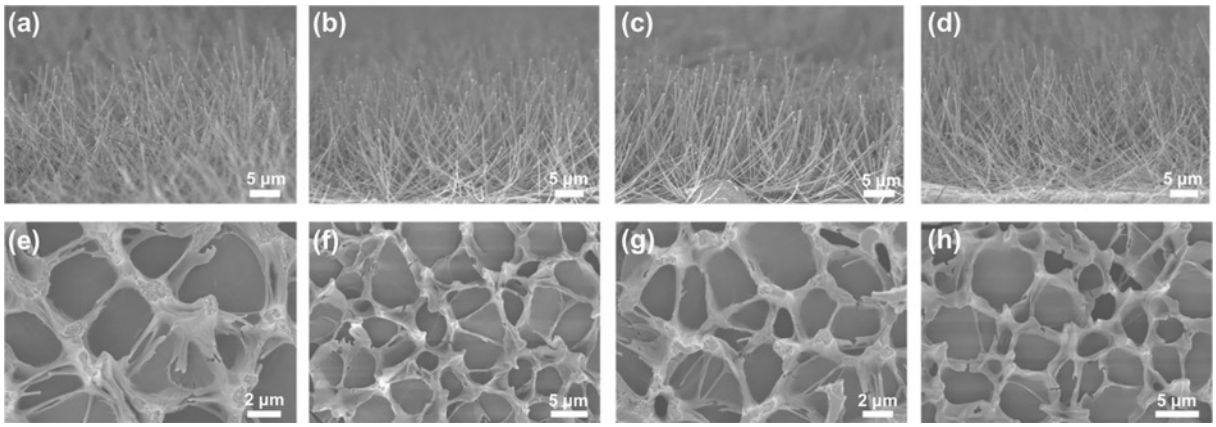

Figure S17. SEM images of the HHAs formed by (a-d) Fmoc-L-FFS, (e-h) Fmoc-L-FWS with different achiral fluorescent molecules in the films: (a, e) TPE, (b, f) thioflavin T, (c, g) coumarin 6, and (d, h) acid red 52, respectively.

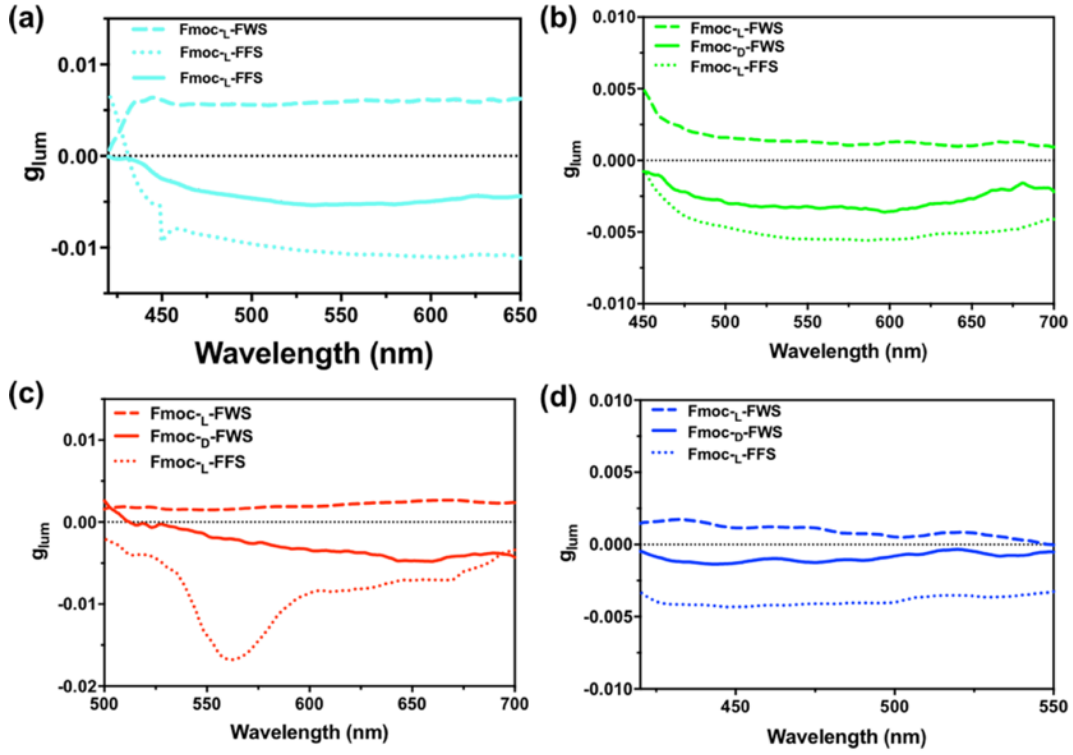

Figure S18. The g_{lum} spectra of the Fmoc-$_L$-FFS, Fmoc-$_L$-FWS, and Fmoc-$_D$-FWS with different dye molecules and AIE molecules: (a) thioflavin T, (b) coumarin 6, (c) acid red 52, and (d) tetraphenylethylene, respectively.

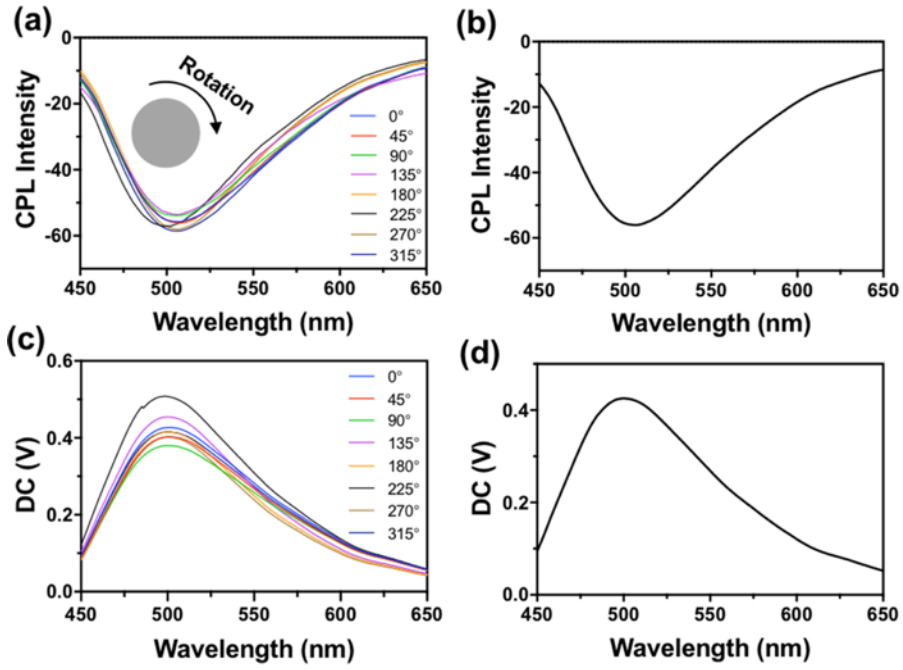

Figure S19. CPL spectra of the Fmoc-$_L$-FFS/THT films. We rotated the quartz plate for 45° clockwise and the data was recollected. After rotating the quartz plate for 8 times, we collected a set of spectra (a). To further eliminate linear dichroism artefacts, the spectra in (a) were then averaged to give a

single CPL curve that was suitable for secondary structural analysis (b). (c, d) DV data during the CPL collection at different wavelength, indicating there were little scattering and absorption artefacts. When the film was rotated by eight angles, there was no obvious difference in the CPL spectrum except for a little intensity difference, indicating that the CPL signal was caused by the chiral arrangement of the achiral fluorescent dyes rather than the polarized emission.

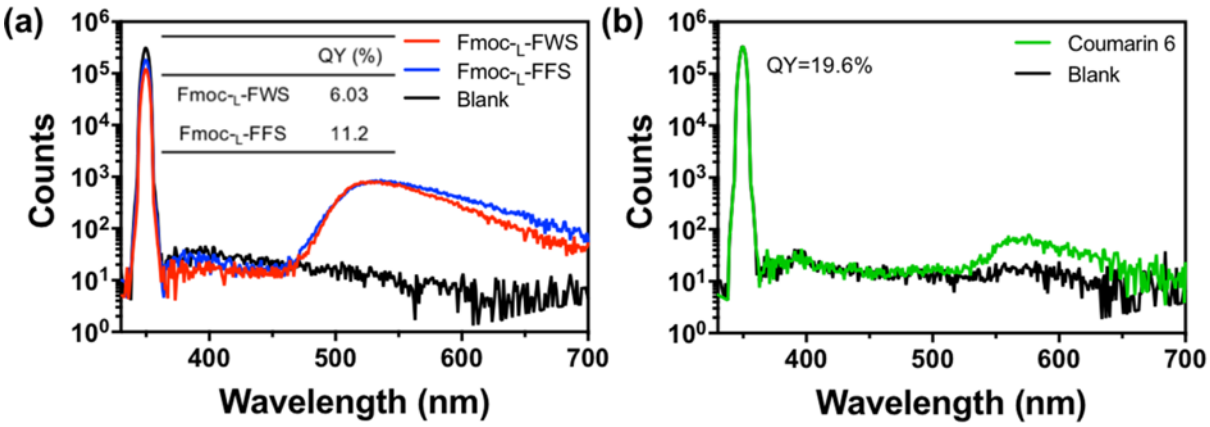

Figure S20. Quantum yields (QYs) of the (a) Fmoc-tripeptides/coumarin 6 films and (b) isolated coumarin 6 solutions.

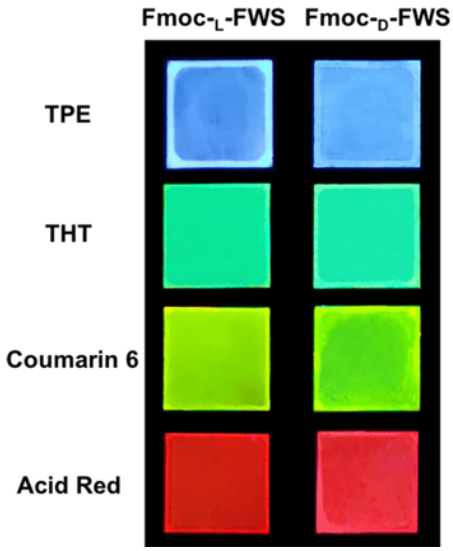

Figure S21. Photographs of the Fmoc-L-FWS, and Fmoc-D-FWS with different different dye molecules and AIE molecules: under irradiation at 365 nm. Blue, blue-green, green, and red CPL were obtained with tetraphenylethylene, thioflavin T, coumarin 6, and acid red 52, respectively.

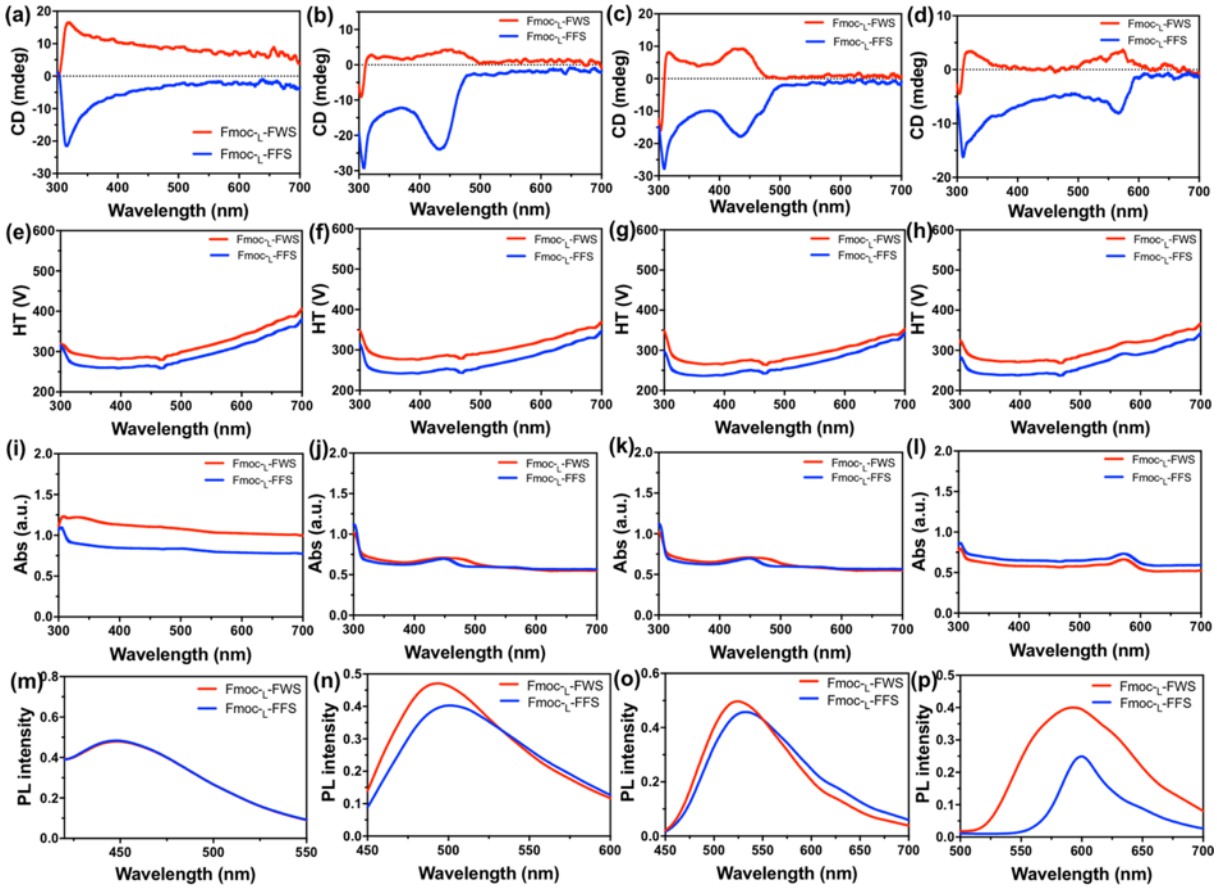

Figure S22. (a-d) CD, (e-h) HT, (i-l) Abs, and (m-p) PL spectra of the Fmoc-L-FFS or Fmoc-L-FWS with different achiral fluorescent molecules: (a, e, i, m) TPE, (b, f, j, n) thioflavin T, (c, g, k, o) coumarin 6, and (d, h, l, p) acid red 52, respectively.

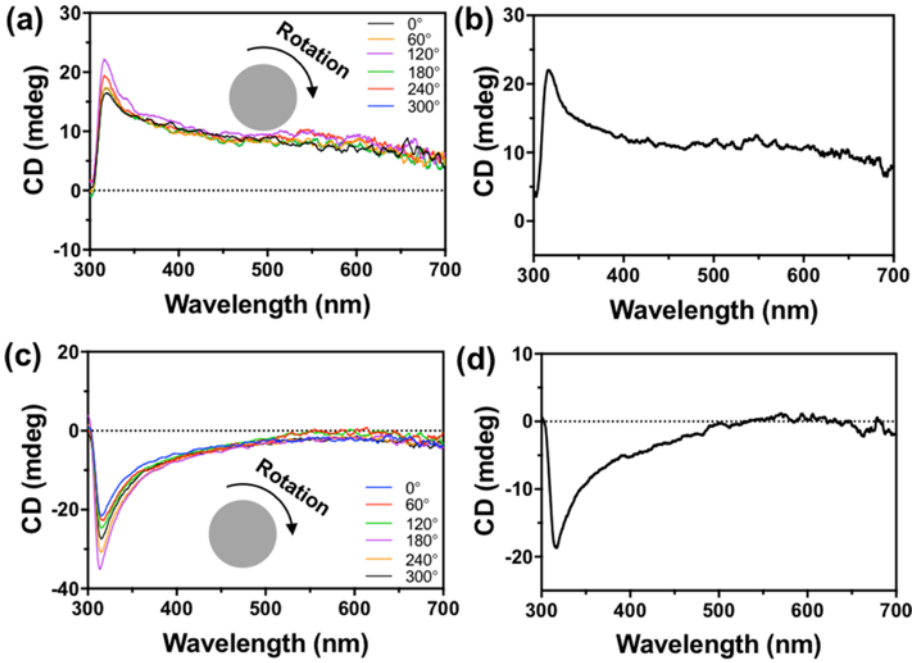

Figure S23. CD spectra of the (a-b) Fmoc-$_L$-FWS/TPE, and (c-d) Fmoc-$_L$-FFS/TPE films. We rotated the quartz plate for 60° clockwise and the data was recollected. After rotating the quartz plate for 6 times (a, c) and flipping the quartz plate (b, d), we collected a set of spectra. When the film was rotated by six angles, there was no obvious difference in the CD spectrum except for a little intensity difference. The results indicated that there were little scattering and absorption artefacts.

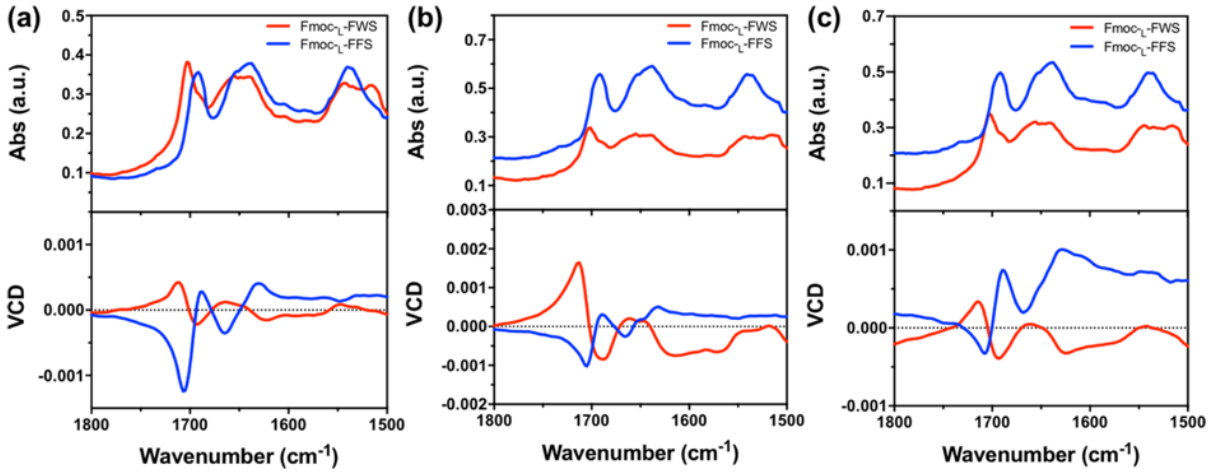

Figure S24. Fourier transform infrared spectroscopy and vibrational circular dichroism spectroscopy of the Fmoc-$_L$-FWS and Fmoc-$_L$-FFS assemblies with different dye molecules in the films: (a) thioflavin T, (b) coumarin 6, and (c) acid red 52, respectively.

Figure S25. Photographs of the Fmoc-L-FWS, and Fmoc-L-FFS aqueous solutions with different fluorescent dyes: (a_1) Fmoc-L-FWS/THT, (a_2) Fmoc-L-FWS/coumarin 6, (a_3) Fmoc-L-FWS/acid red 52, (a_4) Fmoc-L-FFS/THT, (a_5) Fmoc-L-FFS/coumarin 6, (a_6) Fmoc-L-FFS/acid red 52, respectively. The upper images were obtained in room light, and the fluorescent photographs in the second row were obtained under 365 nm UV lamp excitation.

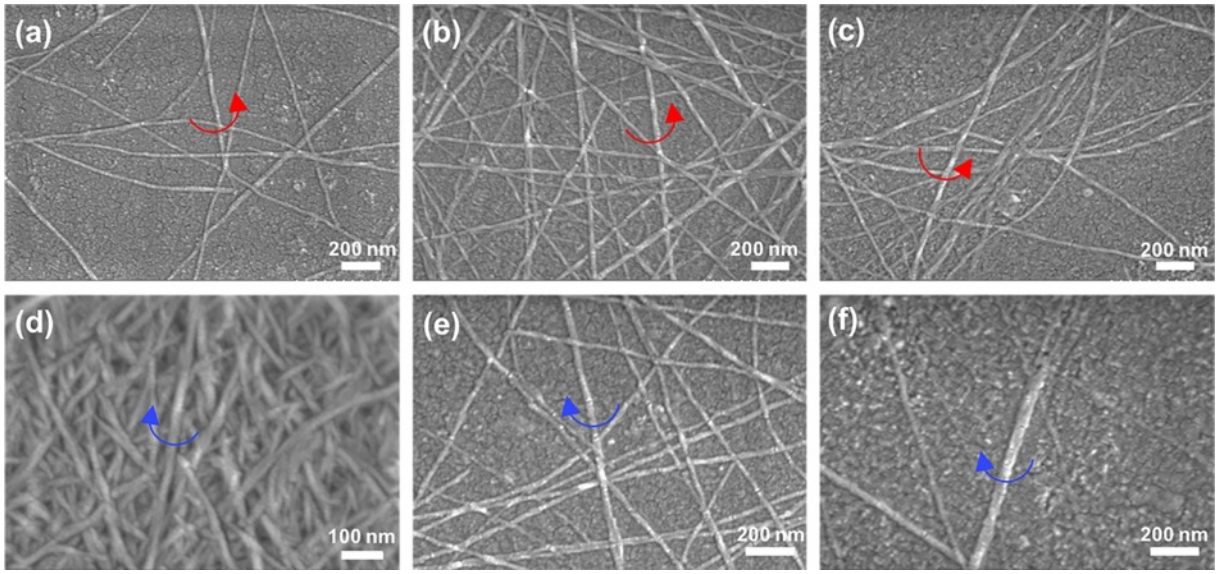

Figure S26. SEM images of the (a-c) Fmoc-L-FWS or (d-f) Fmoc-L-FFS nanohelices with different achiral fluorescent molecules in the aqueous solutions: (a, d) thioflavin T, (b, e) coumarin 6, and (c, f) acid red 52, respectively.

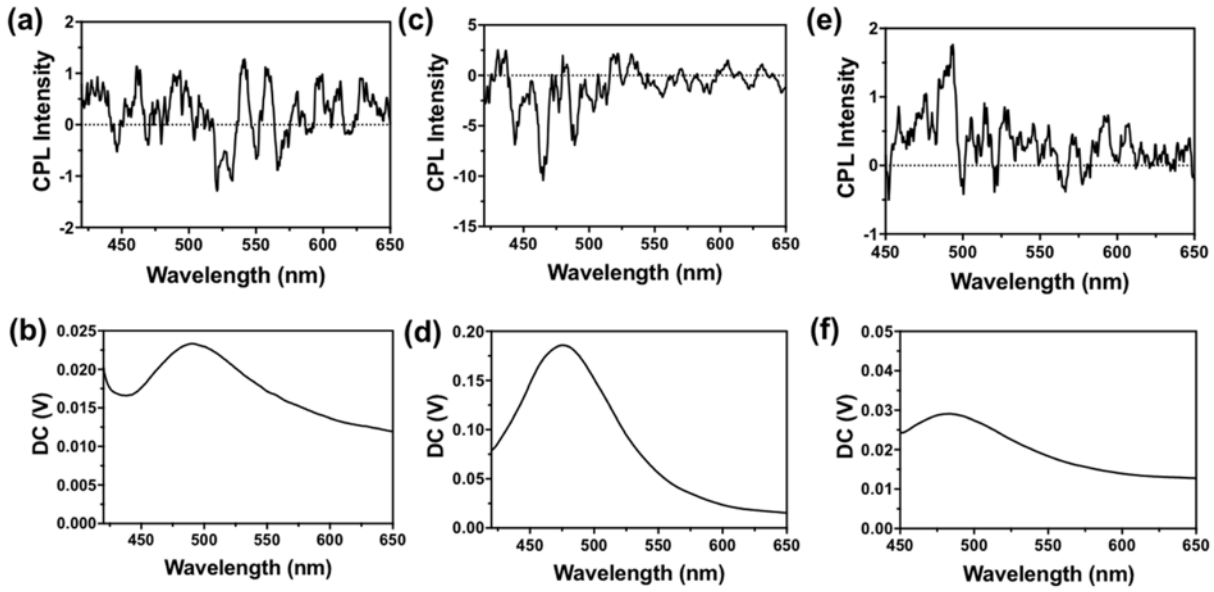

Figure S27. The CPL spectra and DC spectra of the (a) Fmoc-$_{L}$-FWS, (b) Fmoc-$_{D}$-FWS, and (c) Fmoc-$_{L}$-FFS with THT in the aqueous solutions, respectively.

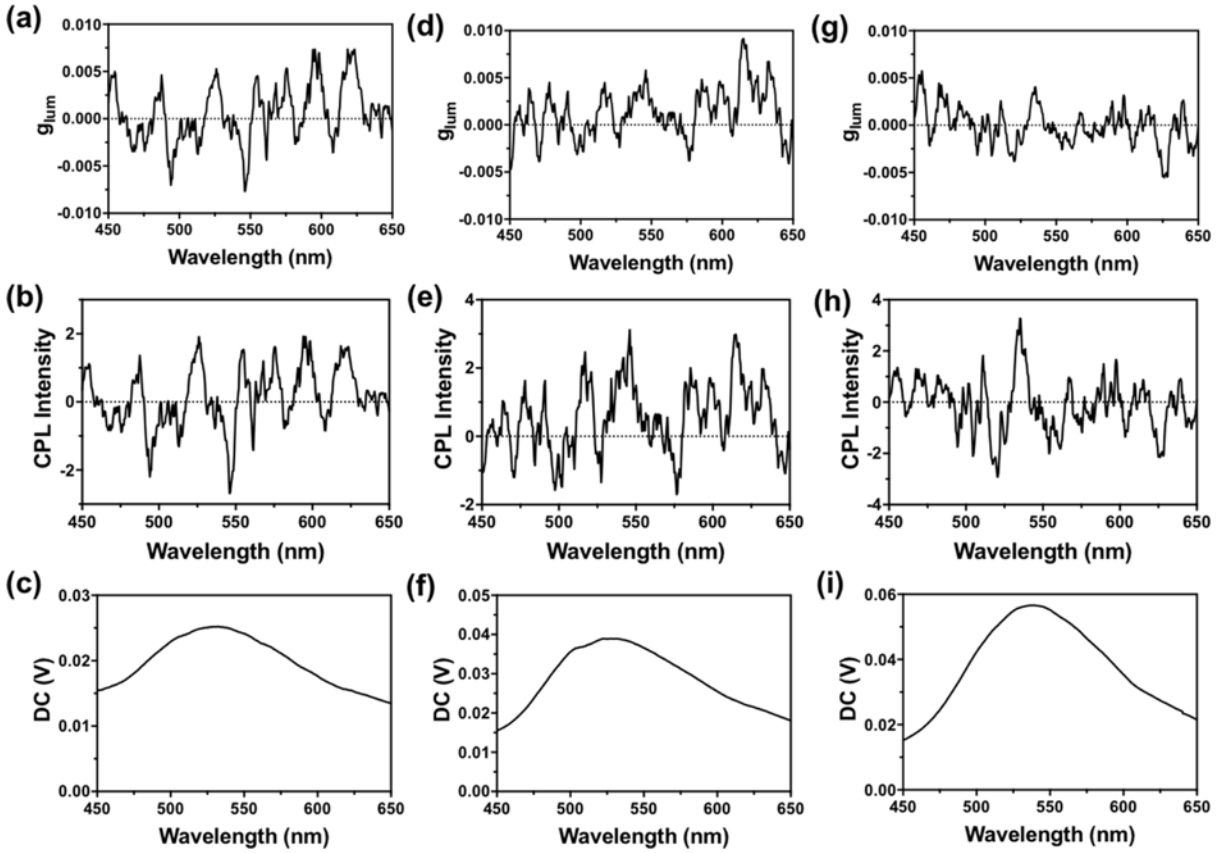

Figure S28. The g_{lum} spectra, CPL spectra, and DC spectra of the (a) Fmoc-$_{L}$-FWS, (b) Fmoc-$_{D}$-FWS, and (c) Fmoc-$_{L}$-FFS with coumarin 6 in the aqueous solutions, respectively.

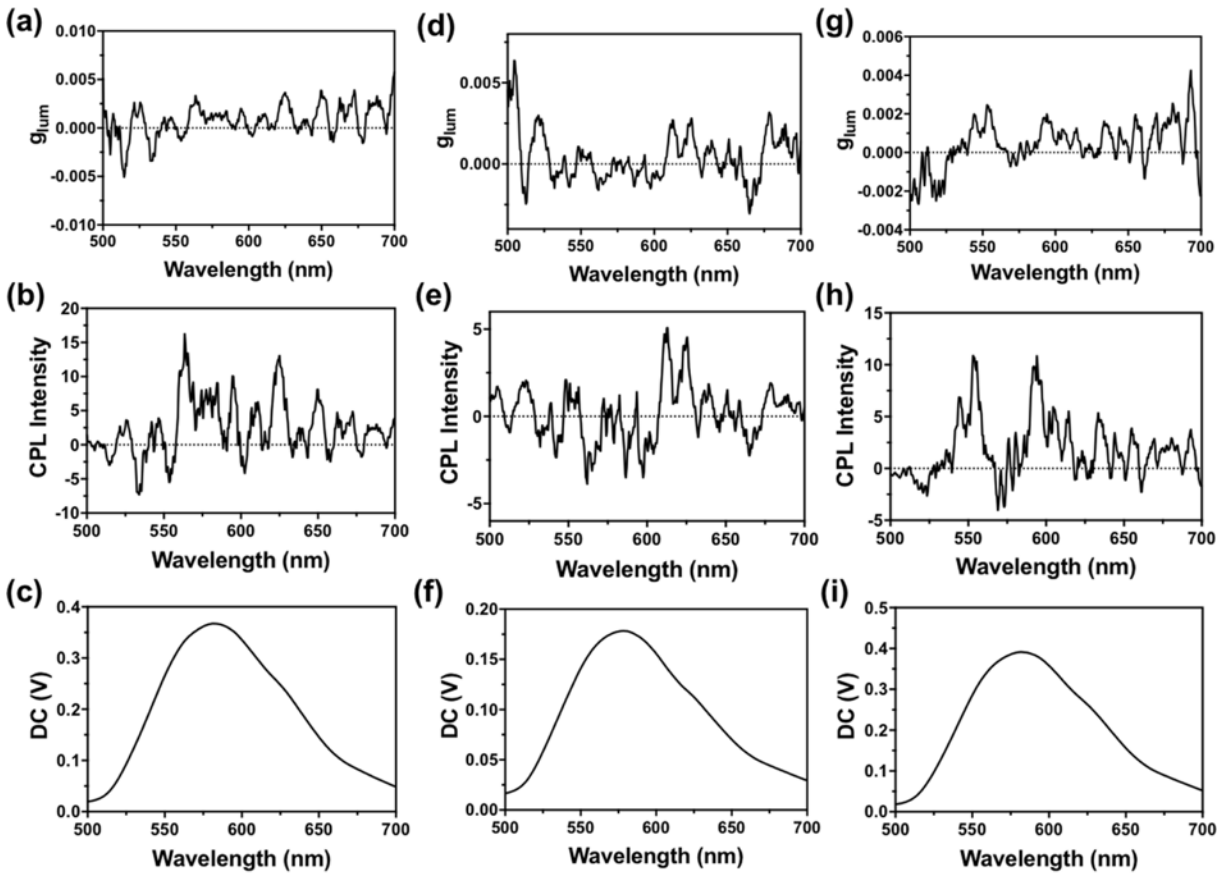

Figure S29. The g_{lum} spectra, CPL spectra, and DC spectra of the (a) Fmoc-$_L$-FWS, (b) Fmoc-$_D$-FWS, and (c) Fmoc-$_L$-FFS with acid red 52 in the aqueous solutions, respectively.

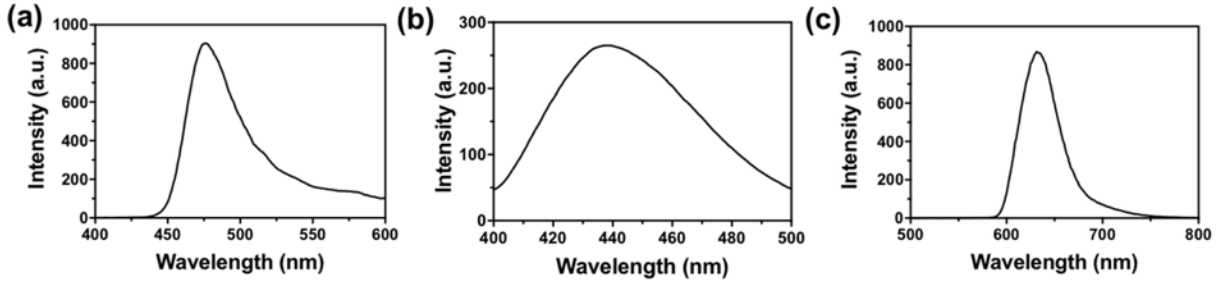

Figure S30. Fluorescence spectra of the dye aqueous solutions: (a) thioflavin T, (b) coumarin 6, and (c) acid red 52, respectively.

References

1. Abraham, M. J.; Murtola, T.; Schulz, R.; Páll, S.; Smith, J. C.; Hess, B.; Lindahl, E., GROMACS: High performance molecular simulations through multi-level parallelism from laptops to supercomputers. *SoftwareX* **2015,** *1-2*, 19-25.
2. Lindorff-Larsen, K.; Piana, S.; Palmo, K.; Maragakis, P.; Klepeis, J. L.; Dror, R. O.; Shaw, D. E., Improved side-chain torsion potentials for the Amber ff99SB protein force field. *Proteins* **2010,** *78*, 1950-8.
3. Schrodinger, LLC, The PyMOL Molecular Graphics System, Version 1.8. 2015.
4. Berendsen, H. J. C.; Postma, J. P. M.; van Gunsteren, W. F.; Hermans, J., Interaction Models for Water in Relation to Protein Hydration. In *Intermolecular Forces: Proceedings of the Fourteenth Jerusalem Symposium on Quantum Chemistry and Biochemistry Held in Jerusalem, Israel, April 13–16,* **1981**, Pullman, B., Ed. Springer Netherlands: Dordrecht, **1981**; pp 331-342.
5. Humphrey, W.; Dalke, A.; Schulten, K., VMD: Visual molecular dynamics. *J. Mol. Graph.* **1996,** *14*, 33-38.
6. de Jong, D. H.; Singh, G.; Bennett, W. F. D.; Arnarez, C.; Wassenaar, T. A.; Schäfer, L. V.; Periole, X.; Tieleman, D. P.; Marrink, S. J., Improved Parameters for the Martini Coarse-Grained Protein Force Field. *J. Chem. Theory Comput.* **2013,** *9*, 687-697.
7. M. J. Frisch, G. W. T., H. B. Schlegel, G. E. Scuseria, M. A. Robb, J. R. Cheeseman, G. Scalmani, V. Barone, G. A. Petersson, H. Nakatsuji, X. Li, M. Caricato, A. Marenich, J. Bloino, B. G. Janesko, R. Gomperts, B. Mennucci, H. P. Hratchian, J. V. Ortiz, A. F. Izmaylov, J. L. Sonnenberg, D. Williams-Young, F. Ding, F. Lipparini, F. Egidi, J. Goings, B. Peng, A. Petrone, T. Henderson, D. Ranasinghe, V. G. Zakrzewski, J. Gao, N. Rega, G. Zheng, W. Liang, M. Hada, M. Ehara, K. Toyota, R. Fukuda, J. Hasegawa, M. Ishida, T. Nakajima, Y. Honda, O. Kitao, H. Nakai, T. Vreven, K. Throssell, J. A. Montgomery, Jr., J. E. Peralta, F. Ogliaro, M. Bearpark, J. J. Heyd, E. Brothers, K. N. Kudin, V. N. Staroverov, T. Keith, R. Kobayashi, J. Normand, K. Raghavachari, A. Rendell, J. C. Burant, S. S. Iyengar, J. Tomasi, M. Cossi, J. M. Millam, M. Klene, C. Adamo, R. Cammi, J. W. Ochterski, R. L. Martin, K. Morokuma, O. Farkas, J. B. Foresman, and D. J. Fox *Gaussian 09*, Revision C.01; Wallingford CT, **2016**.
8. Stephens, P. J.; Devlin, F. J.; Chabalowski, C. F.; Frisch, M. J., Ab Initio Calculation of Vibrational Absorption and Circular Dichroism Spectra Using Density Functional Force Fields. *J. Phys. Chem.* **1994,** *98*, 11623-11627.
9. Petersson, G. A.; Bennett, A.; Tensfeldt, T. G.; Al-Laham, M. A.; Shirley, W. A.; Mantzaris, J., A complete basis set model chemistry. I. The total energies of closed-shell atoms and hydrides of the first-row elements. *J. Chem. Phys.* **1988,** *89*, 2193-2218.

10. Runge, E.; Gross, E. K. U., Density-Functional Theory for Time-Dependent Systems. *Phys. Rev. Lett.* **1984,** *52*, 997-1000.
11. Lu, T.; Chen, F., Multiwfn: a multifunctional wavefunction analyzer. *J. Comput. Chem.* **2012,** *33*, 580-92.